Astron. Astrophys. 295, 423–434 (1995)

ASTRONOMY AND ASTROPHYSICS

Shell lines in disks around Be stars

I. Simple approximations for Keplerian disks*

R.W. Hanuschik[1,2]

[1] Astronomisches Institut, Universität Tübingen, Waldhäuser Str. 64, D-72076 Tübingen, Germany
[2] Astronomisches Institut, Ruhr-Universität Bochum, Postfach 10 21 48, D-44780 Bochum, Germany

Received 26 May 1994 / Accepted 25 July 1994

Abstract. This paper investigates so-called shell absorption lines occurring in Be star disks seen edge-on. These lines are counterparts of absorption troughs in P Cyg-type profiles for different geometry and kinematics and offer a probe of a small portion of the circumstellar disk. Contrary to other studies, this investigation concentrates on Fe lines as prototype examples for metallic shell lines, which have an extremely small thermal width (2 km s^{-1} at 10^4 K). However, it is also demonstrated that incorporation of turbulence provides a powerful tool to generalize the results towards lines from arbitrary ions.

As a simple, though not unphysical model, a purely Keplerian, isothermal disk in hydrodynamic equilibrium is adopted. The intention of this paper is to provide simple approximations for easy use. Simple geometrical illustrations of the shell absorption behaviour projected onto the stellar disk are used to illustrate the origin of shell line profiles.

It is shown that resulting Fe shell profiles consist of a broad *kinematic* part and a narrow *thermal* core, the narrowness of which depends on the intrinsic Doppler width of the line. The outer disk radius R_d may cause, under certain circumstances, cusps at radial velocities $\pm V_d = R_d^{-3/2}$. These cusps can become the deepest points in the line profile, thus causing a central peak. Finally it is demonstrated that if the disk becomes turbulent, the central peak disappears, and the Fe shell profiles are identical to hydrogenic lines from non-turbulent disks.

This study is intended to provide tools for comparison to recent high-resolution, high-S/N measurements of optical shell lines in Be stars. However, it also bears significance for the more general case of central continuum light sources partly occulted by thin disks.

Key words: line: profiles – stars: Be – accretion disks – circumstellar matter

Send offprint requests to: R.W. Hanuschik, Tübingen address

* Based on observations obtained at the European Southern Observatory, La Silla, Chile

1. Introduction

Be stars are rapidly rotating B-type stars with an at least transiently existing circumstellar envelope emitting line radiation in the optical range, superposed onto the photospheric spectrum. The width of these emission lines clearly correlates with the width of photospheric absorption lines (Hanuschik 1989). Therefore the circumstellar envelope must possess cylindric symmetry with its polar axis coinciding with the rotational axis of the star. More specifically, the envelope must be a rather thin disk because stellar light directed towards the observer is not absorbed by the disk in most cases.

At high inclination, often quite narrow absorption lines are observed in addition, with central intensity well below the stellar continuum. These absorption lines are termed shell lines. Though some authors believe that circumstellar envelopes around Be stars showing shell lines are physically different from those merely exhibiting pure emission lines (e.g. Doazan 1987), it seems much more likely that shell lines are a simply perspective effect. If at high inclination lines of sight from the observer towards the central star intersect parts of the disk which is cooler than the stellar photosphere, shell-type absorption will occur; if not (i.e. at lower inclination), pure emission is observed. This simple geometric model does not contradict the observed transition of a few stars from "shell-type" to "Be-type" spectra or vice versa (e.g. *o* And, HR 1180, 59 Cyg: Dachs 1987 and references therein) because the crucial phenomenon of intersection may, in a certain narrow inclination range, critically depend upon the effective outer disk radius if the disk is concave-shaped (see Sect. 2.2). In the following we will therefore regard shell lines as a purely geometrical effect.

Shell lines are counterparts of the absorption trough in P Cygni-type line profiles, for the case of Keplerian rotation instead of stellar wind outflow, and of disk-like rather than spherical geometry (Fig. 1). Like absorption troughs in P Cygni-type profiles, shell lines offer a probe of the kinematics and density conditions in a small part of the circumstellar envelope, i.e. in that part which appears projected onto the stellar surface as seen from the observer. For inclination $i = 90°$, this part occupies a

fraction $\approx 2R_\star R_d/(\pi {R_d}^2) = 2R_\star/(\pi R_d)$ where R_d is the outer disk radius and $R_\star$ the stellar radius. This fraction becomes $\approx 1/8$ for the case $R_d = 5R_\star$, and $\approx 1/16$ for $R_d = 10R_\star$. *This is the smallest fraction of a Be star disk which can be investigated spectroscopically* in absence of an eclipsing companion.

Though shell lines offer a considerable diagnostic potential for studying physical conditions in Be star disks, their profiles have apparently not received much interest. Kogure (1975) and Hirata & Kogure (1978) have studied hydrogen shell lines, focusing on the Balmer progression and central depth, while Higurashi & Hirata (1978) have also investigated parameters of metallic shell lines. However, there appears to exist no detailed study of the impact of kinematics, geometry and density law on shell profiles. Such study appears even more desirable in view of the high-resolution, high-S/N data which have become available in the meantime (e.g., Hanuschik et al. 1988, Slettebak et al. 1992, Dachs et al. 1992).

For a study of Be star envelope conditions, metallic shell lines are preferrable over hydrogen shell lines because of their lower intrinsic width. Especially, Fe II shell lines are most favourable because they show up frequently in optical spectra of Be stars, and because their thermal broadening (Doppler width) is only of order 2 km s^{-1}, compared to, e.g., 13 km s^{-1} in case of hydrogen lines at 10^4 K. For this reason, Fe II shell lines are very sensitive tracers of kinematical conditions in Be star envelopes. In this paper, the origin of shell lines in a simple, though not unphysical Be star disk model will be investigated. Some simple analytical approximations for shell line profiles in Keplerian disks will be presented, in order to provide tools for easy analysis of observations. In a following paper, numerical models for more complicated kinematics will be presented which, e.g., can be used to investigate asymmetric line profiles. Furthermore comparison to observed line profiles will be undertaken there.

2. Basic equations

2.1. Optical depth and geometry

In a gross and somewhat oversimplified sense, Sobolev (1960) has already treated the problem of shell line profiles in his pioneering book *Moving envelopes of stars*. His Fig. 4 presents results for the limiting case of infinite radial extent of the envelope, inclination 90°, no vertical extension of the shell, and for some mixtures of expansion and rotational velocities. He obtained, for the case of pure rotation, a triangular profile shape with depth 0.5. This line contour is readily understood (see Sect. 5). However, it is not observed. The reason therefore is, as we will show, an oversimplification of the physical situation and leads us to regard a more physical model for the circumstellar envelope here.

The more realistic physics here will include the kinematics and the vertical structure of the disk. These two parameters are crucial for the shape of shell lines. Other parameters will be treated here in an ad hoc, though not unreasonable sense.

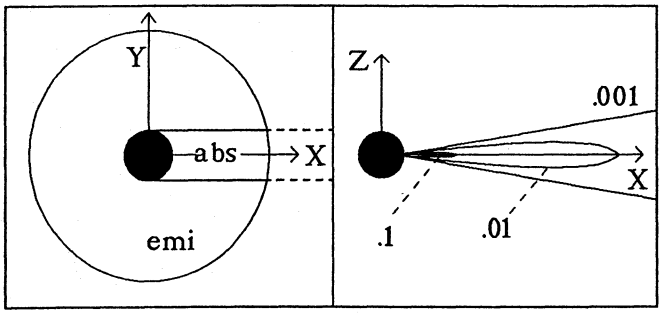

Fig. 1. Sketch of Be disk geometry; *abs*, *emi* = parts of disk where shell absorption and emission takes place. Density contours are labelled with their value of N/N_0 [Eq.(5)]

In an earlier study of symmetric Fe II emission lines in Be stars, Hanuschik (1989) has shown that the typical width of optically thin emission lines is about $2\ v \sin i$ where v denotes the stellar rotational velocity measured from the width of photospheric absorption lines. Statistically Be stars rotate close to their break-up velocity, i.e. $v = \gamma v_{\rm crit} = \gamma\sqrt{GM_\star/R_\star}$ with $\gamma \approx$ 0.8–1. Then, if particle motion in the envelope is of the same magnitude, it must be *gravitationally dominated*. Since infall is excluded from the frequently observed symmetry of optically thick emission lines, e.g. of Hα (e.g. Hanuschik et al. 1988), matter in the envelope must be rotating, i.e. we are dealing with a simple centrifugally supported *Keplerian disk*. Furthermore this disk is likely to be a thin one because the average half opening angle has been found to be as small as 12° (Hanuschik 1994).

Shell line absorption will be treated in the following as a process of absorption of stellar radiation by the circumstellar disk, thus disregarding reemission. This is justified because in a Keplerian disk large Doppler gradients exist making the reemission process extremely anisotropic. Like in the more familiar accretion disks (the structure of which resembles that of Be star disks very much), there is an extremely anisotropic escape probability of line photons, being much larger in directions within the disk plane, at angles $\approx 45°$ to the line of sight, than radially outwards or perpendicular to the disk plane (Horne & Marsh 1986; Hummel & Dachs 1992).

Let us use a cartesian coordinate system (X, Y, Z) with (X, Y) defining the equatorial disk plane (Fig. 1, right part). We assume the observer to look into the equatorial plane along the X-axis. All coordinates will be expressed in units of stellar radius $R_\star$, with $X \equiv x/R_\star$ etc. We start from the standard definition of optical depth τ_V at some radial velocity $V \equiv v_{\rm rad}/v_{\rm K}(1)$ along an arbitrary ray parallel to the X-axis,

$$\tau_V(Y, Z) = R_\star \int_{X_{\rm min}}^{X_{\rm max}} \kappa_V N_{\rm l}\, {\rm d}X\ , \qquad (1)$$

where $v_{\rm K}(1)$ denotes the Keplerian velocity at $R = 1$. (We note that the normalization to $v_{\rm K}(1)$ is natural in a Keplerian disk

and does not imply any assumption about the *stellar* rotational velocity.) The absorption coefficient is given by

$$\kappa_V = \frac{\pi e^2}{mc} f \Phi_V \frac{\lambda_o}{V_{\kappa(1)}}, \quad (2)$$

where f is the oscillator strength and Φ_V the local absorption profile. N_l is the number density in the lower state of this transition. For sake of simplicity, let us assume in the following that $N_l = \beta_l \cdot N$, with β_l = const. and N the number density of all particles. (In general, β_l would take the excitation and ionization conditions in the disk into account.)

2.2. Density law

Besides the kinematics, the second important input into our disk model comes from the observation that Be star disks, though sometimes rapidly variable, may be at times constant, i.e. in a quasistationary state, over years. As the dynamic (rotational) timescale is of the order of days, this means that for Be star disks a hydrostatic equilibrium (in vertical direction) is possible. We will assume such equilibrium in the following. Then the density law $N(R, Z)$ in the disk becomes

$$N(R, Z) = N'(R) \cdot \exp\left\{-\frac{1}{2}\left(\frac{Z}{H(R)}\right)^2\right\}, \quad (3)$$

which is the standard form for a disk in hydrostatic equilibrium in Z-direction (Pringle 1981). Here we have introduced the radius coordinate in the equatorial plane, $R \equiv (X^2 + Y^2)^{1/2}$. $H(R) = h(R)/R_\star$ is the normalized vertical scale height,

$$H(R) = C_s \cdot R^{3/2}, \quad (4)$$

where $C_s \equiv c_s/v_K(R_\star)$ is the isothermal sound speed. In the following, we consider an isothermal disk with temperature T_d = 10 000 K so that c_s = 12.7 km s^{-1}. For the central B-type star we adopt $M_\star = 10 M_\odot$ and $R_\star = 7 R_\odot$ yielding $v_K(R_\star)$ = 521 km s^{-1}.

Adopting an ad hoc power law with index α and $N'(1) \equiv N_0$ for the radial density distribution $N'(R)$, we obtain

$$N(R, Z) = N_0 R^{-\alpha} \exp\left\{-\frac{1}{2}\frac{Z^2}{C_s^2 R^3}\right\}. \quad (5)$$

We furthermore assume that the disk extends from the stellar surface (R = 1) out to some outer radius R_d.

Figure 1 (right part) shows density contours N/N_0 = 0.1, 0.01, 0.001 for this density law. The resulting disk is concavely shaped and basically identical in structure to a thin accretion disk, the thinness provided by the condition $H(R) \ll R$ which is easily satisfied within $R_d \lesssim 1000 R_\star$.

2.3. Local absorption profile

The local absorption profile Φ_V is required to obey $\int_{-\infty}^{+\infty} \Phi_V dV$ = 1 and will be assumed to be Gaussian, i.e.

$$\Phi_V(X, Y, Z) = Q \exp\left\{-\frac{1}{2}\left(\frac{V - V_{rad}(X, Y, Z)}{\Delta V_D}\right)^2\right\}, \quad (6)$$

with $Q = (\sqrt{2\pi}\Delta V_D)^{-1}$. All radial velocities are normalized as before. For the moment, the Doppler width ΔV_D of the local line profile is assumed to be solely due to thermal broadening, thus neglecting turbulent motion along the line of sight. This assumption clearly yields a minimum Doppler width which has the advantage that effects due the intrinsic line broadening and those due to large-scale kinematic broadening can be most efficiently distinguished. Any additional contribution to ΔV_D by turbulence will broaden and flatten the local line profile accordingly. Turbulence will be incorporated in Sect. 6.

The thermal Doppler width for Fe lines at 10^4 K is $\Delta V_D = (2kT/\mu m_p)^{1/2}/v_K(R_\star)$ = 1.7 km s^{-1}/521 km s^{-1}= 3.3 10^{-3}, and $Q = (\sqrt{2\pi}\Delta V_D)^{-1}$ = 120.89.

2.4. General expression for shell line optical depth

Using Eqs. (5) and (6), we can now rewrite Eq. (1) and obtain

$$\tau_V(Y, Z) = \tau_0 Q \int_{X_{min}}^{X_{max}} R^{-\alpha} \exp\left\{-\frac{1}{2}\left(\frac{Z}{C_s X^{3/2}}\right)^2 - \frac{1}{2}\left(\frac{V - V_{rad}(X, Y, Z)}{\Delta V_D}\right)^2\right\} dX, \quad (7)$$

with

$$\tau_0 = \frac{\pi e^2}{mc} f \frac{\lambda_o}{V_{\kappa(1)}} \beta_l N_0 R_\star. \quad (8)$$

We note a useful analytical simplification, viz. the two physically independent Gaussians from the density law N and the local line profile Φ_V effectively merge into a single new Gaussian.

The shell line profile $F_V/F_\star$ can now be obtained by integrating Eq. (7) across the whole stellar disk, i.e.

$$F_V/F_\star = \frac{1}{\pi}\int_{-1}^{+1}\int_{-\sqrt{1-Z^2}}^{+\sqrt{1-Z^2}} \exp\{-\tau_V(Y, Z)\} dY dZ. \quad (9)$$

We will disregard limb darkening in the following as it is not expected to considerably influence the line profiles.

2.5. Strategy for calculating the approximate shell line profile

Let us divide the approach to calculate the shell line into three parts: first, the central depth will be determined; second, the line profile value at a critical point will be calculated, and third, expressions will be derived at intermediate radial velocities. The form of the velocity field plays a central rôle in this analysis. Because of the assumption of hydrostatic equilibrium, the Z-component of radial velocity vanishes and the velocity field is a function of X, Y only. Then its form strongly affects the optical depth structure in the *equatorial* plane of a Keplerian disk, but not within a *meridional* plane. It is therefore useful to treat these two cases separately in the following.

3. Central depth of shell lines

3.1. Meridional plane

In the meridional plane through stellar centre and observer ($Y = 0$), the slope of optical depth $\tau_{V=0}(Y=0, Z)$ is governed by the Z-dependence of the density law alone, and Eq. (7) reads

$$\tau_{V=0}(Z) = \tau_0 Q \int_1^{R_d} X^{-\alpha} \exp\left\{-\frac{Z^2}{2C_s^2 X^3}\right\} dX$$
$$= \tau_0 Q \cdot \Gamma_\alpha(Z, R_d)\,, \qquad (10)$$

where R_d is the outer disk radius and has replaced, for obvious reasons, the formal upper integration limit ∞. The two terms on the right-hand side of Eq. (10) are easy to interpret: $\tau_0 Q = \pi e^2/mc \cdot f\beta_1 N_0 R_\star Q$ contains only parameters which are constants for our problem and can be treated together as scaling factor, while Γ_α is a term depending only on the density law.

In the absence of velocity gradients in the equatorial plane, shell absorption would cause a horizontal black bar projected onto the stellar disk. The vertical half-width of this bar is well approximated and visualized by the *equivalent height* H_{sh} of the absorbing disk. This parameter takes a central rôle in our analysis and describes a stellar disk being totally black up to height H_{sh}. Starting from the expression for the Z-integration in Eq. (9), we set

$$\int_0^1 \exp\{-\tau(Z, R_d)\}\, dZ = 1 - H_{sh}\,. \qquad (11)$$

This integral will be solved here for two practically relevant density laws, $\alpha = 2$ and 4. For $\alpha = 4$, the density integral Γ_4 in Eq. (10) can be solved analytically. Substituting $\rho := X^{-3}$ and integrating between R_d^{-3} and 1, we obtain

$$\Gamma_4(Z, R_d) = \frac{1}{3} \cdot \frac{2C_s^2}{Z^2} [E(\rho_1) - E(\rho_2)] \qquad Z \neq 0,$$
$$= \frac{1}{3} \cdot (\rho_2 - \rho_1) \qquad Z = 0\,, \qquad (12)$$

with $E(\rho) = \exp\{-Z^2\rho/(2C_s^2)\}$ and $\rho_1 = R_d^{-3}$, $\rho_2 = 1$.

Similar solutions can be found for $\alpha = 7, 10$ etc., but are practically unimportant since line fits have shown that in Be star disks, $\alpha \lesssim 4$ (Hanuschik 1988). Therefore $\alpha = 4$ can be considered as limiting value.

In the next step, numerical integration of $\exp\{-\tau_0 Q \cdot \Gamma_4\}$ according to Eq. (11) yields H_{sh} for $\alpha = 4$.

For $\alpha = 2$, H_{sh} is approximated by setting

$$\exp[-\tau(H_{sh})] \stackrel{!}{=} 1/2 \qquad (13)$$

and solving for H_{sh} iteratively by numerical integration of Eq. (10). This procedure has been performed as a test for the case $\alpha = 4$ as well and has shown very good agreement of the result obtained by both methods.

H_{sh} has been calculated for parameter values $\alpha = 2$ and 4, $R_d = 5$, 10, 20, and $\tau_0 = 10^{-1}$ ... 10^7. The results are collected in Table 1 and depicted in Fig. 2. Because H_{sh} is defined by the disk's geometry, it can become larger than 1. Of course, absorption stops at $H_{sh} = 1$, but for certain interpolating approximations in Sect. 4 these geometrical values are useful. They are given in brackets in Table 1. For disk radius $R_d = 5$, H_{sh} increases only very slowly with τ_0 because it is of the order of the vertical scale height H which is only 0.27 at R_d. For $R_d = 10$ and 20, this scale height is of the order of 1 and the density slope is much shallower along the lines of sight. Therefore $H_{sh} = 1$ is approached at rather low values of τ_0 (less than 1 for $\alpha = 2$, 10 for $\alpha = 4$).

Table 1. Equivalent shell height H_{sh} for Fe shell lines

τ_0	H_{sh}^a					
	$\alpha = 2$			$\alpha = 4$		
	$R_d = 5$	10	20	$R_d = 5$	10	20
10^{-2}	0.039	0.052	0.059	0	0	0
$10^{-1.5}$	0.128	0.199	0.265	0.040	0.041	0.041
10^{-1}	0.253	0.494	0.848	0.082	0.084	0.084
1	0.506	(1.23)	(2.87)	0.226	0.259	0.265
10	0.718	(1.86)	(4.76)	0.443	0.692	0.814
10^2	0.898	(2.39)	(6.35)	0.654	(1.31)	(2.12)
10^3	(1.06)	(2.85)	(7.70)	0.839	(1.90)	(3.88)
10^4	(1.20)	(3.27)	(8.90)	1.00	(2.42)	(5.54)
10^5	(1.32)	(3.63)	(9.98)	(1.15)	(2.87)	(6.97)

[a] Values in brackets (= $H_{sh}^\star$) are used for interpolation (Sect. 4.2)

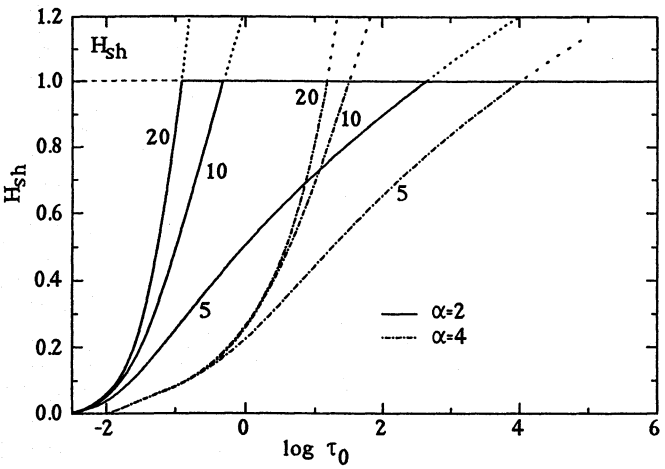

Fig. 2. Equivalent shell height H_{sh} for Fe lines and disk radii $R_d = 5$, 10, 20, optical depths $\tau_0 = 10^{-2}$ ... 10^5 and density laws $\alpha = 2, 4$

3.2. Equatorial plane

Up to now, we have neglected the fact that, though a considerable fraction of material in front of the star is seen at radial velocity $v_{rad} = 0$ in a Keplerian disk, this value is not strictly valid for the whole projected part of the disk. As velocity gradients are

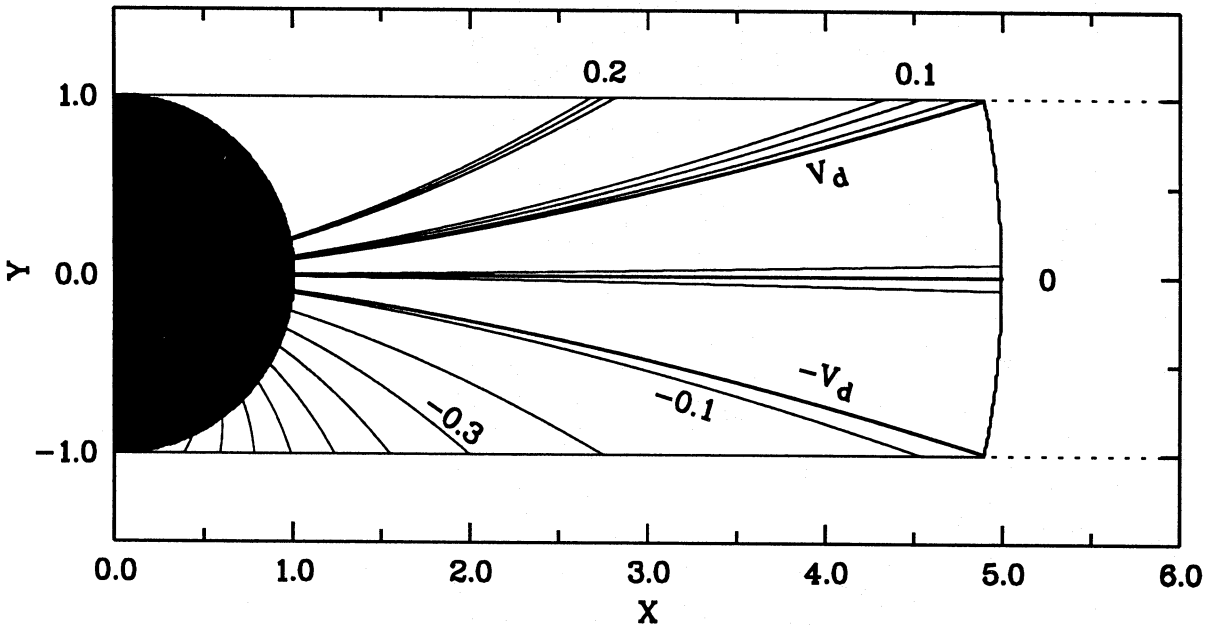

Fig. 3. Radial velocity contours in (X, Y)-plane in the region of shell absorption ($Y = -1 \ldots + 1$). Velocity contours $V = -0.9, -0.8 \ldots + 0.2$ are shown; in case of $V = 0$, 0.1, 0.2, the corresponding contours $\pm 2\Delta V_D$ are also shown. Furthermore the critical velocity $\pm V_d = R_d^{-3/2}$ is plotted for the case $R_d = 5$ (thicker line). The disk rotates counterclockwise

very efficient in reducing optical depth of a given shell (Sobolev approximation), we now must take this effect into account.

With the X-axis in the direction towards the observer (Fig. 1, left part), the radial velocity field $V_{rad} \equiv v_{rad}/v_K(R_\star)$ in the disk plane is given by

$$V_{rad}(X, Y) = R^{-1/2} \cdot \frac{Y}{R} = Y \cdot (X^2 + Y^2)^{-3/4} \qquad (14)$$

(Fig. 3). Here, like throughout the paper, counter-clockwise rotation is assumed. The coordinate equation for a specific radial velocity contour V is

$$\begin{aligned} X_V(Y) &= \left[(Y/V)^{4/3} - Y^2\right]^{1/2} && V \neq 0 \\ Y &= 0 && V = 0\,. \end{aligned} \qquad (15)$$

Equation (7) now reads, with $Z = 0$, $V = 0$ and V_{rad} from Eq. (14),

$$\begin{aligned} \tau_{V=0}(Y) &= \tau_0 Q \int_1^{R_d} R^{-\alpha} \exp\left\{-\frac{1}{2}\left(\frac{Y}{\Delta V_D X^{3/2}}\right)^2\right\} \mathrm{d}X \\ &= \tau_0 Q \cdot \Lambda_\alpha(Y, R_d)\,, \end{aligned} \qquad (16)$$

where Λ_α describes the X-integration of the density law with the local line broadening function as weight factor. According to this broadening profile, only those particles in the disk plane with radial velocities within a few Doppler widths around 0 effectively contribute to absorption.

The contribution of Eq. (16) to the line profile is obtained by integrating $\exp[-\tau(Y)]$ across Y. We note that $\tau(Y)$ is formally very similar to $\tau(Z)$ in Eq. (10), a consequence of the Gaussian shapes of both the Z-component of the density law and the Y-component of the line broadening function for $V = 0$. We therefore solve the absorption integral in a similar fashion, defining the *effective absorption width* Y_{eff} for radial velocity 0 in the equatorial plane, with

$$\int_0^1 \exp\{-\tau(Y, R_d)\}\,\mathrm{d}Y = 1 - Y_{eff}\,. \qquad (17)$$

Again, for $\alpha = 4$ an analytical solution for $\tau_0 Q \cdot \Lambda_4$ is available,

$$\begin{aligned} \Lambda_4(Y, R_d) &= \frac{1}{3} \cdot \frac{2\Delta V_D^2}{Y^2}\left[F(\rho_1) - F(\rho_2)\right] && Y \neq 0, \\ &= \frac{1}{3} \cdot (\rho_2 - \rho_1) && Y = 0\,, \end{aligned} \qquad (18)$$

with $F(\rho) = \exp\{-Y^2\rho/(2\Delta V_D^2)\}$ and ρ_1, ρ_2 as in Eq. (12).

For $\alpha = 2$, Y_{eff} is approximated by

$$\exp[-\tau(Y_{eff})] \stackrel{!}{=} 1/2\,.$$

Y_{eff} is tabulated in Table 2 and depicted in Fig. 4 for the same range of parameters as H_{sh}. Because of the much smaller intrinsic width of the Gaussian (ΔV_D instead of C_s), Y_{eff} remains much smaller than H_{sh}. Its typical scale is given by the projection of the Doppler width ΔV_D at R_d onto the stellar disk, $Y_D = \Delta V_D R_d^{3/2} = 0.037, 0.104, 0.295$ for $R_d = 5, 10, 20$. Y_{eff} is between 1.5 Y_D ($\tau_0 = 1$) and 5.5 Y_D ($\tau_0 = 10^7$).

3.3. Central depth

We are now in the position to calculate the central depth of a shell line for the most extreme case, $i = 90°$ (edge-on view). We can

Table 2. Equivalent absorption width $Y_{\rm eff}$ for Fe shell lines

τ_0	$Y_{\rm eff}$					
	$\alpha = 2$			$\alpha = 4$		
	$R_{\rm d} = 5$	10	20	$R_{\rm d} = 5$	10	20
10^{-1}	0.034	0.066	0.115	0.012	0.014	0.024
1	0.068	0.165	0.382	0.030	0.040	0.050
10	0.096	0.255	0.637	0.062	0.102	0.136
10^2	0.120	0.320	0.848	0.090	0.182	0.309
10^3	0.141	0.382	1	0.110	0.260	0.537
10^4	0.160	0.436	1	0.135	0.328	0.752
10^5	0.177	0.486	1	0.160	0.388	0.926
10^6	0.193	0.531	1	0.175	0.442	1
10^7	0.207	0.574	1	0.190	0.491	1

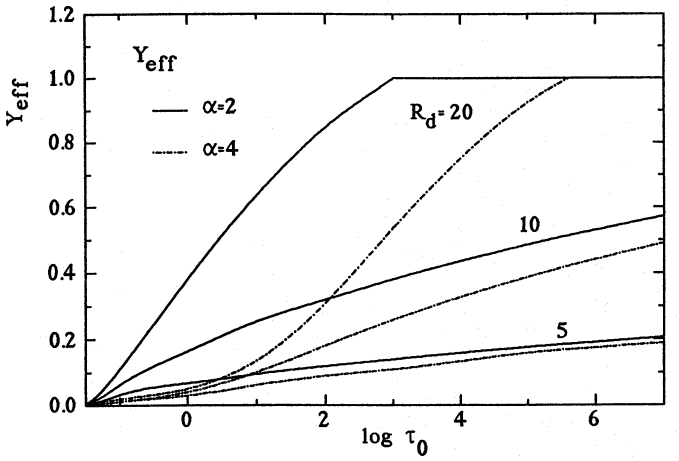

Fig. 4. Effective absorption width $Y_{\rm eff}$ for same parameter values as in Fig. 2

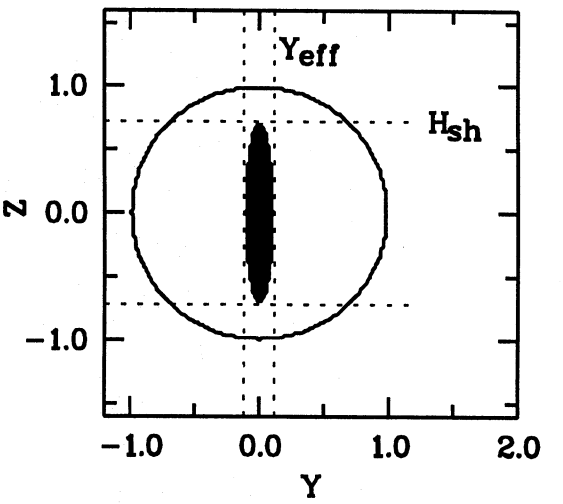

Fig. 5. Sketch of obscured area projected onto the stellar disk, for V=0

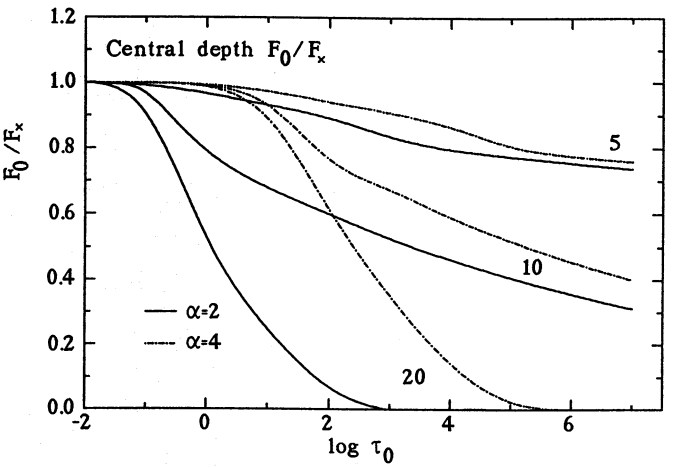

Fig. 6. Central depth $F(V = 0)$ of Fe lines for model parameters as in Fig. 2

make full use of the analytical simplification noted earlier that optical depth $\tau(Y, Z)$ is a function of two independent Gaussians in Z and Y. If we insert Eq. (14) into Eq. (7), we obtain for $V = 0$:

$$\tau_V(Y,Z) = \tau_0 Q \int_1^{R_{\rm d}} R^{-\alpha} \exp\left\{-\frac{1}{2}\sigma^2\right\} {\rm d}X \ , \qquad (19)$$

with

$$\sigma^2(X,Y,Z) = \sigma_Y^2 + \sigma_Z^2 = X^{-3}\Delta V_{\rm D}^{-2}\left(\frac{Z^2}{A} + Y^2\right) \ . \qquad (20)$$

Here we have used $\Delta V_{\rm D}^2 = C_{\rm s}^2/A$, with $A = 56$ for Fe. Integrating Eq. (19) across the stellar disk will effectively yield a black ellipse with major halfaxis $H_{\rm sh}$ and minor halfaxis $Y_{\rm eff}$ (Fig. 5), and the central depth of a shell line in a Keplerian disk is

$$F(V = 0)/F_\star = 1 - H_{\rm sh} \cdot Y_{\rm eff} \ . \qquad (21)$$

For Fe lines, $Y_{\rm eff}$ will be much smaller than $H_{\rm sh}$ because $\sigma_Z = \sqrt{56}\,\sigma_Y$.

For saturated $H_{\rm sh}$,

$$F(V = 0)/F_\star = 1 - \frac{4}{\pi}\int_0^{Y_{\rm eff}} \sqrt{1 - Y^2}\,{\rm d}Y \ . \qquad (22)$$

is a better representation for central depth.

Figure 6 shows the resulting central depth for the same parameter values as in Fig. 2. For disk radii $R_{\rm d} \leq 5$, central intensity of Fe shell lines cannot be deeper than about 0.75 even at very high optical depth. For $R_{\rm d} = 10$, considerable depth is obtained at $\tau_0 > 1$, while for $R_{\rm d} = 20$ Fe lines can even become totally black at $\tau_0 > 10^2$ for $\alpha = 2$, and at $\tau_0 > 10^5$ for $\alpha = 4$.

4. Line profile outside $V = 0$

4.1. Critical velocity $V_{\rm d}$

The central depth of a shell line from a Keplerian disk is determined, as we have seen, by *thermal broadening*, $\Delta V_{\rm D}$ (if turbulence is absent). For contours $V \neq 0$, we are entering a

different regime because now the inclination of radial velocity contours against the line of sight becomes important. This is the regime of *kinematic broadening*.

Apart from the contour $V = 0$, there is one other especially noteworthy velocity contour, defined by the specific geometry of the problem: the critical radial velocity V_d,

$$V_d = \pm R_d^{-3/2} \; . \tag{23}$$

This is the contour that intersects in the equatorial plane both the outer disk radius R_d and the shell absorption limit $Y = \pm 1$ (Fig. 3). This contour is the *longest one in the shell volume, and it covers the largest range of Y-values across the stellar disk*, starting from $Y = R_d^{-3/2}$ and extending to $Y = 1$.

In order to obtain the line depth at V_d, we follow the same strategy as in the preceding section, i.e. we determine the geometrical shape of the obscured area projected onto the stellar disk. The width of this area is approximately given by

$$\Delta Y(V = V_d) \approx 1 - V_d \; . \tag{24}$$

The shape is no more ellipsoidal but trapezium-like, vertically limited by the values of H_{sh} for $Y = 1$ and $Y = V_d$, resp. For $Y = 1$, H_{sh} is identical to the value for $V = 0$ as tabulated in Table 1. This vertical limit has to be replaced, for larger values of H_{sh}, by the corresponding segment of the outer rim of the stellar disk. For $Y = V_d$, H_{sh} is of the order of the scale height H of the disk for $R = 1$. According to Eq. (4), the scale height at $R = 1$ is only 0.024, thus we may simply set $H_{sh}(R = 1) = 0$. The obscured area can now be well approximated by $\arctan H^\star_{sh} - H^\star_{sh} V^2$ (Fig. 7), where $H^\star_{sh}$ stands for the bracketed values for H_{sh} in Table 1 in case that $H_{sh} > 1$. The line profile value for $V = V_d$ becomes

$$F(V_d)/F_\star \approx 1 - \frac{\arctan H^\star_{sh} - H^\star_{sh} V_d^2}{\pi} \; . \tag{25}$$

We note that the central depth $F(0)$ and the depth at the critical velocity depend on different parameters: $1 - F(0)/F_\star = H_{sh} \cdot Y_{eff}$, while $1 - F(V_d)/F_\star \propto H^\star_{sh}(1 - V_d^2)$. While Y_{eff} depends on the disk extension and optical depth τ_0, V_d depends only on geometry. This leads to the fact that under certain circumstances the line profile may become deeper at V_d than at $V = 0$ (see below).

4.2. The case $V \geq V_d$

For $V \geq V_d$, we can easily generalize the previous case. In the equatorial plane, absorption for radial velocity contour V is only possible in the range

$$\Delta Y(V \geq V_d) = 1 - V \tag{26}$$

simply on geometrical grounds. The projected absorption area is again approximately trapezium-shaped, with outer height $2H_{sh}(V)$ and inner height $2VH_{sh}(V)$. The outer limitation $2H_{sh}(V)$ is to be replaced by the rim of the stellar disk. $H_{sh}(V)$

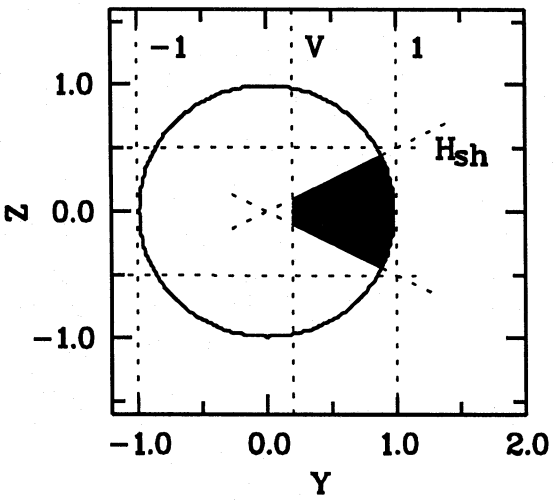

Fig. 7. Like Fig. 5, for the case $V \geq V_d$

is the effective height for shell absorption at $X_V(1)$, the X-coordinate where the contour V intersects the shell limit $Y = 1$ (Fig. 3). A sufficiently correct procedure to obtain $H_{sh}(V)$ is to simply scale $H^\star_{sh}(R_d)$ by setting $H_{sh}(V) = H^\star_{sh}(R_d) \cdot X_V(1)/R_d$ and use Eq. (15) for $X_V(1)$:

$$H_{sh}(V) \approx H^\star_{sh} \frac{(V^{-4/3} - 1)^{1/2}}{R_d} \; . \tag{27}$$

For the line profile we find

$$F(V \geq V_d)/F_\star \approx 1 - \frac{\arctan H_{sh}(V) - H_{sh}(V) \cdot V^2}{\pi} \tag{28}$$

with $H_{sh}(V)$ from the previous equation. Because of the interpolation for $H_{sh}(V)$, this approximation becomes less and less accurate for larger radius. This affects, however, only velocities smaller than V_d and is not a serious problem.

4.3. The case $0 < V \leq V_d$

Here, the Y-range capable of obscuration is given by $V...V \cdot R_d^{3/2}$ [see Fig. 3 and Eq. (14) with $X = R_d$]. For $H_{sh} < 1$ (i.e. small disk radii and $\tau_0 \leq 10^3$) the obscuration region is a triangle of area $H_{sh} V(R_d^{3/2} - 1)$. Thus,

$$F(0 < V \leq V_d)/F_\star \approx 1 - \frac{H_{sh}}{\pi} V(R_d^{3/2} - 1) \; .$$

For $H_{sh} > 1$, however, the shape becomes more complicated and is not well approximated by this equation. Here an even simpler procedure yields satisfying results for two reasons: first, the condition $H_{sh} > 1$ falls together with the condition $R_d > 5$ which implies very small V_d. Second, the whole approximation breaks together anyway when V becomes of the order of ΔV_D, i.e. very close to $V = 0$, because then kinematical broadening has to be replaced by thermal broadening. Thus an appropriate

procedure for the region $0 \le V \le V_d$ in case that $H_{sh} > 1$ is to linearly interpolate between $F(V = V_d)$ and $F(V = 0)$,

$$F(0 < V \le V_d)/F_\star \approx 1 - H_{sh}Y_{eff} + \frac{V}{V_d}[H_{sh}Y_{eff} - \pi^{-1} \arctan H^\star_{sh}] \; . \quad (29)$$

5. Results for non-turbulent disks

Let us now collect the results for metallic shell line profiles from non-turbulent Keplerian disks in hydrostatic equilibrium [Eqs. (21, 25, 28, 29)]:

$$F_V/F_\star \approx \begin{cases} 1 - H_{sh} \cdot Y_{eff} & V = 0 \\ 1 - H_{sh} \cdot Y_{eff} + \frac{V}{V_d}[H_{sh}Y_{eff} - \pi^{-1} \arctan H^\star_{sh}] & 0 < V \le V_d \\ 1 - \frac{H^\star_{sh}}{\pi}\left(\frac{\arctan H^\star_{sh}}{H^\star_{sh}} - V^2\right) & V = V_d \\ 1 - \frac{H_{sh}(V)}{\pi}\left(\frac{\arctan H_{sh}(V)}{H_{sh}(V)} - V^2\right) & V \ge V_d \end{cases} \quad (30)$$

with $H_{sh}(V)$ from Eq. (27). Because at increasingly larger R_d only velocities $V < V_d(R_d)$ have contours within the shell volume, one should use the expression for $V \ge V_d$ and $R_d = 5$ for all radii $R_d \ge 5$.

A representative collection of calculated shell profiles from Eq. (30), all for the case $\Delta V_D = 0.0033$ (Fe lines), are depicted in Fig. 8. As mentioned earlier, these results are only approximative and intended (*i*) to enable a semi-quantitative discussion of shell line profiles from Keplerian disks, and (*ii*) to provide easy-to-handle analytical expressions for comparison to observations. A precise numerical analysis will be published later (paper II, in prep.).

In all graphs of Fig. 8, the parameter combination $R_d = 5, \tau_0 = 10, \alpha = 2$ has been chosen as standard model. In Fig. 8a, the impact of varying τ_0 (= 1...10^3) is shown. These profiles are very similar to each other and especially all show a typical central peak and sharp cusps at V_d. Figure 8b shows the standard profile with increasing outer disk radius R_d = 5, 10, 20. With increasing R_d, the central reversal becomes less pronounced, and is replaced, at $R_d = 20$, by the deep thermal core with central intensity $F(0)/F_\star = 0.363$. For $R_d > 20$, central intensity 0 is reached. In Fig. 8c, the density law is varied. Steeper density gradients cause a flatter profile, with the overall shape remaining unchanged. Finally, Fig. 8d shows a comparison of the standard profile to an exact numerical calculation. Noticeable differences occur only in the flanks of the profile and are due to the rough interpolation of $H_{sh}(V)$ in Eq. (27). Central intensity, intensity at the critical velocities and the shape of the central peak are almost exactly reproduced by our analytical approximation.

In general, the resulting profiles show the following properties:

1. Symmetry. Due to the symmetry of the Keplerian velocity field, all shell profiles are necessarily symmetric.

2. Central peak. Many line profiles show sharp cusps at $\pm V_d$ and a central peak. This rather unexpected peak is a consequence of the caustic-like behaviour of absorption by the $V = 0$ contour: because it is aligned precisely towards the observer, it has very high column density, but occults only a very small fraction of the stellar disk (lighthouse effect). Other contours, though with lower column density, are more efficient in eclipsing parts of the stellar disk. This is especially true for the critical velocity V_d.

A plot of the obscured area for different radial velocities provides additional insight into the mechanism causing the profile shape (Fig. 9). This plot shows $\exp[-\tau(Y, Z)]$ across the stellar disk and has been calculated by numerical integration of Eq. (7). For large radial velocities, the trapezoidal shape of the absorption region is clearly visible, with its area increasing roughly as $(1 - V^2) \cdot V^{-2/3}$. For $V > V_d$, the radial velocity contours leave the shell volume at $Y = 1$. For $V = V_d$, this limit is replaced by R_d, and maximum vertical extension of the obscured region is reached (H_{sh}), as well as maximum horizontal extension $(1 - V_d)$. For smaller radial velocities, the horizontal extent becomes smaller again, and line depth decreases proportionally to V. Central depth in a disk with finite R_d would be 1 if not, at $V \approx \Delta V_D$, the *kinematical* broadening would be replaced by *thermal* broadening which lets $F(0)/F_\star = 1 - Y_{eff}H_{sh}$ and projects an elliptical shadow onto the stellar disk.

Now it is clear that the central peak will always occur if the domain of thermal broadening does not extend beyond $\pm V_d$. This is the case if (*i*) opacity is low, (*ii*) outer disk radius is small, or (*iii*) thermal width is small, especially in absence of turbulence and for species with high atomic weight like iron. The second point is clearly visible in Fig. 8b where the central peak disappears for $R_d \ge 20$. For hydrogen lines (and Fe lines in a turbulent disk), the third point is violated. Their thermal core easily extends beyond V_d and no central peak is to be expected (see next section).

3. Thermal core. A precise limit for the thermal core can be derived introducing the *thermal core velocity* V_{thc},

$$V_{thc} = Y_{eff} R_d^{-3/2} \quad (31)$$

(Fig. 9a). The thermal core then extends between $-V_{thc}$ and $+V_{thc}$. Typical values for V_{thc} of Fe lines are 2–6 Y_{eff} = 0.007–0.020 (Sect. 3.2). Within this radial velocity range, the whole shell volume acts like a static medium, i.e. an interstellar gas cloud. If τ_0 and R_d are sufficienetly high to permit $F_0/F_\star < F_{V_d}/F_\star$, a narrow central depression occurs of typical width V_{thc}, i.e. of order of 0.01–0.02 for Fe lines.

4. Cusps. If cusps at $\pm V_d$ are visible, they carry information about R_d. They correspond to the double peaks in emission-line profiles which arise from the longest radial velocity contour in the emission region ($V_p = R_d^{-1/2}$, see Huang 1972). Here, $V_d = R_d^{-3/2}$.

5. Line wings. For increasing radii R_d, the line wings beyond V_d do not change any more. Thus computations for larger radii can be restricted to the line core.

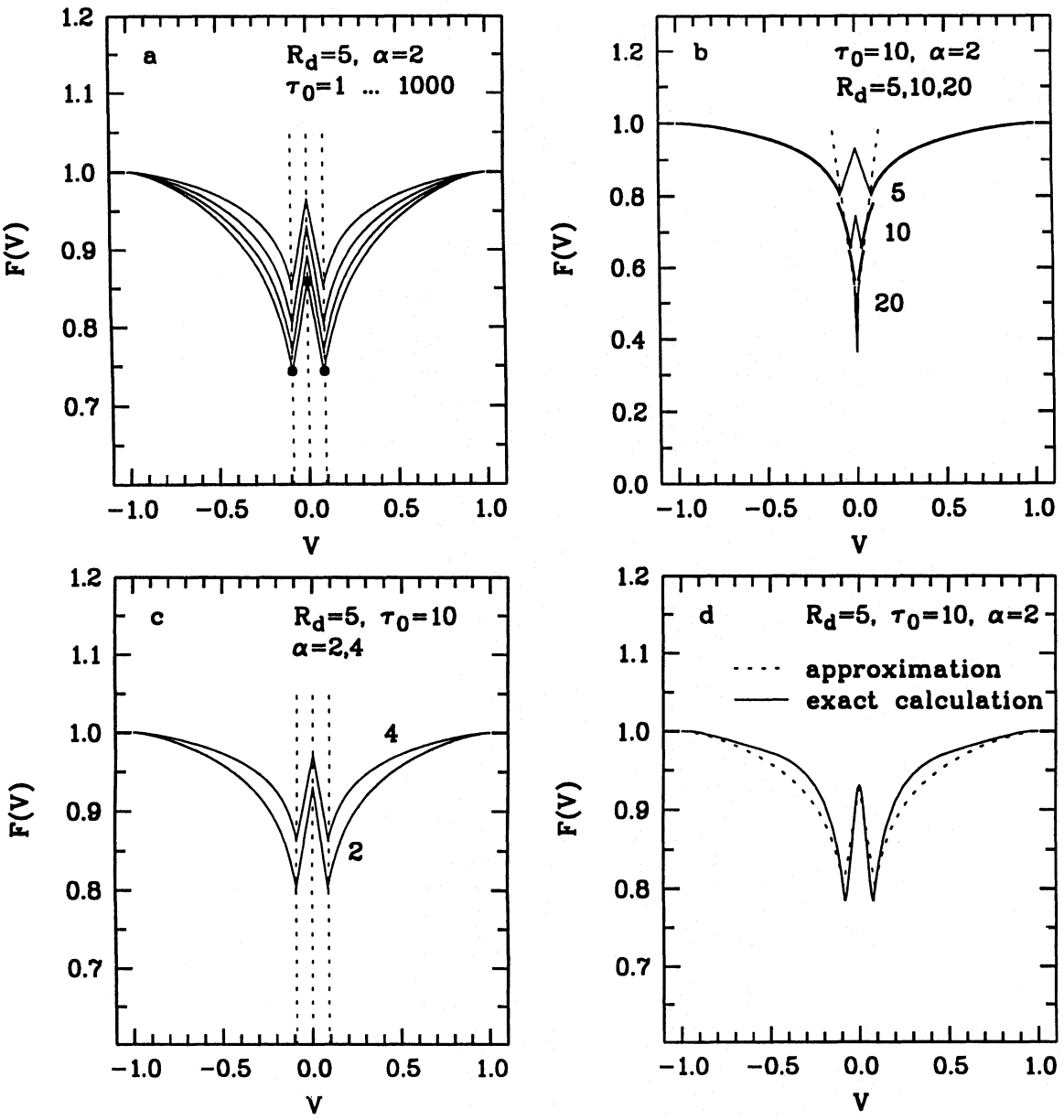

Fig. 8. Approximative shell profiles for hydrostatic, isothermal Keplerian disks around Be stars. **a** Profiles for varying τ_0 (= 1...10^3 from top to bottom; $R_d = 5, \alpha = 2$). Full points mark central intensity $F(0)$ and intensity at critical point, $F(V_d)$, for the case $\tau_0 = 10^3$. Dotted lines indicate $V = 0$ and $\pm V_d$. **b** Profiles for varying outer disk radius ($R_d = 5, 10, 20$; $\tau_0 = 10, \alpha = 2$). Thick line: profile part for $|V| > V_d$, thin line: $|V| < V_d$. The dotted line indicates the asymptotic ($R_d \to \infty$) kinematical part of the shell profile, with central depth 0.5. The imperfect overlap of the respective central parts of the profiles is caused by the approximative character of Eq. (28). **c** Profiles for varying density index ($\alpha = 2, 4$; $\tau_0 = 10, R_d = 5$). **d** Comparison of exact numerical calculation (paper II, in prep.) and approximative profile (this paper), for the standard model

6. Asymptotic kinematical profile. Because thermal and kinematical broadening are independent of each other, very large outer disk radii result in a narrow, deep *thermal* absorption core embedded into a relatively broad and shallow *kinematical* absorption feature. The asymptotic shape of the kinematical part of the shell profile ($V \geq V_d$) can be found by evolving Eq. (28) for $V_d \to 0\,(R_d \to \infty)$, yielding $F_V/F_\star \to 1 - \pi^{-1} \arctan H^\star_{sh}(V_d)$. With $H^\star_{sh}(R_d) \approx 3.6 H(R_d) = 3.6 C_s/V_d$ for $\tau_0 = 10^3$, we obtain

$$F_V/F_\star \to 1/2 + 3.8 V_d \; . \qquad (32)$$

For different values of τ_0, the factor 3.8 becomes slightly different. In any case, central depth in the asymptotic case without thermal broadening becomes 0.5 and the shape of the central profile region is triangular (cf. Fig. 8b).

It is interesting to compare this asymptotic result to Sobolev's (1960) shell profile. He has only regarded the shell contribution in the equatorial plane, thus his model effectively corresponds to a disk with *constant* height h and a square of width h as stellar surface. The asymptotic result ($\tau_0 \to \infty$) for

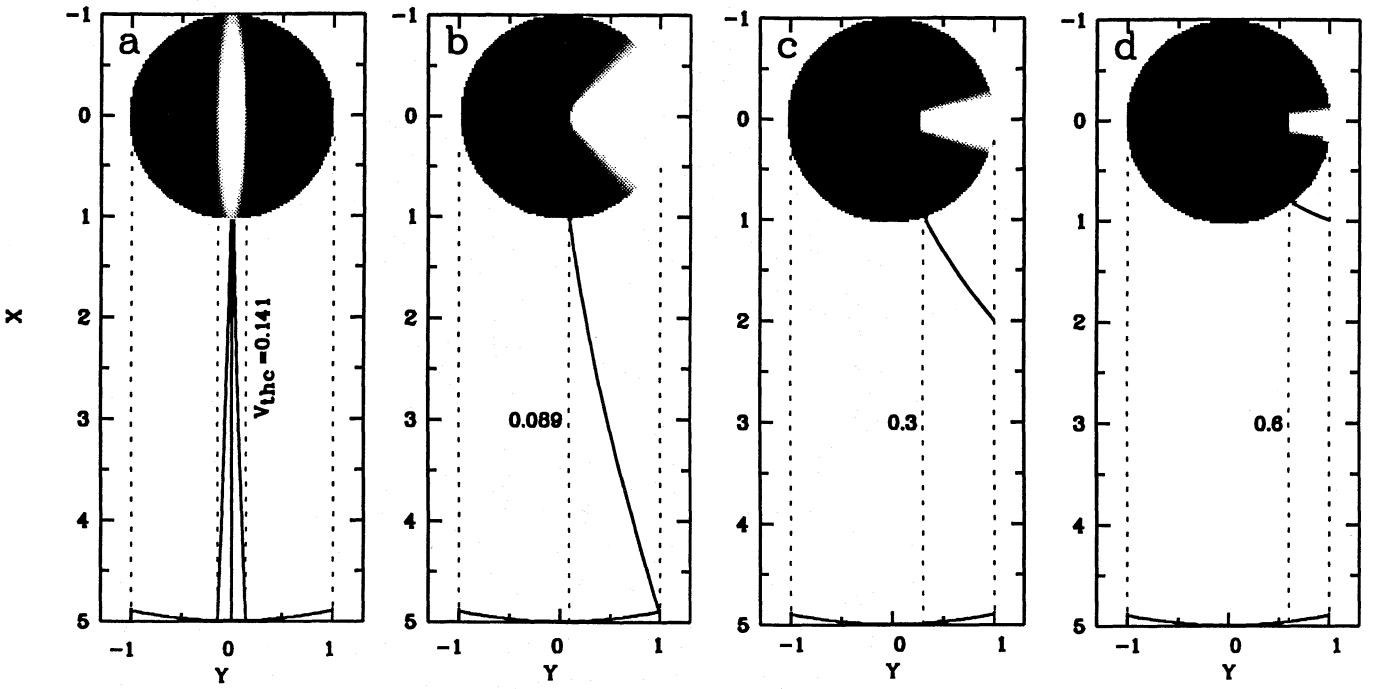

Fig. 9a–d. Region on stellar disk obscured by shell absorption. From **a** to **d**, radial velocities V=0,= 0.089 = V_d, = 0.3, and = 0.6 are shown. In each subgraph, the stellar disk is visible as (Y, Z)-plot like in Figs. 5 and 7, with the obscured area shown white. In addition, the corresponding radial velocity contour is drawn in the (X, Y)-plane, in a manner similar to Fig. 3 apart from a 90° rotation. For $V = 0$, three contours are drawn: $V = -V_{thc}, 0, +V_{thc}$. Vertical dotted lines mark $Y = \pm 1$, $Y = V$, and $Y = \pm V_{thc}$ (for $V = 0$ only)

this model is a triangular profile, $F_V/F_\star = 1/2 + V/2$. We note that the difference in flank shape to our results is due to the different geometry. In addition, the non-appearance of the "thermal peak" of the shell line around $V = 0$ in Sobolev's calculation is completely due to the neglect of thermal broadening.

6. Turbulent disks

As final model parameter, let us now investigate the impact of turbulence onto the line profile. This effect increases the Doppler width and therefore should become important within the thermal core of the shell profile. If $V_{turb} \equiv v_{turb}/v_K(1)$ denotes the amount of turbulent velocity, the Doppler width becomes $\Delta V'_D = \sqrt{\Delta V_{th}^2 + V_{turb}^2}$. In the following, the primed quantities denote those with turbulence included. Thin disks are likely to become turbulent because the Reynolds number for molecular viscosity takes very high values (Frank et al. 1992, pp. 61). This turbulent viscosity is characterized by the scale of the largest eddies, $\lambda_{turb} \approx H$, and the turnover velocity v_{turb} which is not expected to exceed the isothermal sound speed, C_s, as otherwise thermalization by shocks will set in. We will use here these well-known results from accretion disks as well.

Let us parametrize $V_{turb} = \beta C_s$ ($\beta \leq 1$) and investigate the limiting case $\beta = 1$. We find

$$\Delta V'_D = \sqrt{C_s^2(A^{-1} + \beta^2)} \approx C_s\beta \qquad (33)$$

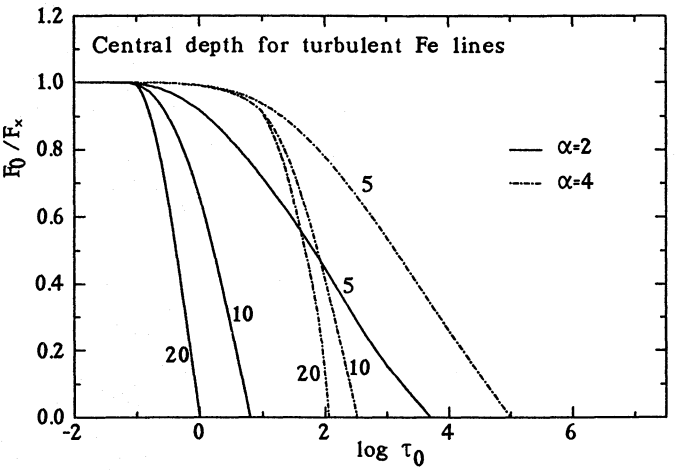

Fig. 10. Central depth $F(V = 0)$ of fully turbulent ($\beta = 1$) Fe lines for model parameters as in Fig. 2

for Fe ($A = 56$). The local absorption profile Φ'_V is still formally the same as in Eq. (6). However, because the relation $Q' = (\sqrt{2\pi}\Delta V'_D)^{-1} < Q$ holds, the profile becomes flatter, and because of $\Delta V'_D > \Delta V_D$, broader than the intrinsic absorption profile without turbulence. Since now $\Delta V'_D \approx C_s$, the two Gaussians in Eq. (7) are the same for $V = 0$, and the obscuration area becomes a *circle of radius* H'_{sh} where $H'_{sh} < H_{sh}$. Values for H'_{sh} are collected in Table 3. They may also be derived from Fig. 2 using the relation $H'_{sh}(\tau_0, Q') = H_{sh}(\tau_0 \frac{Q'}{Q}, Q)$.

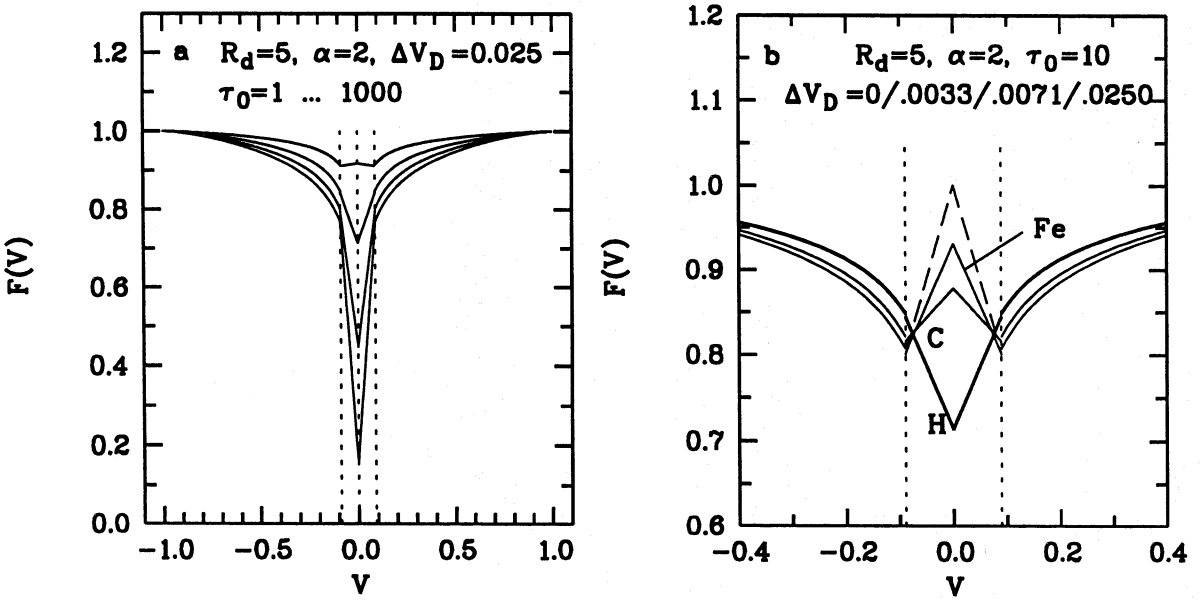

Fig. 11. Approximative shell profiles for turbulent Keplerian disks around Be stars. **a** Fe line profiles for varying τ_0 (= $1...10^3$ from top to bottom; $R_d = 5, \alpha = 2$). As before, dotted lines indicate $V = 0$ and $\pm V_d$. Fully developed turbulence ($\beta = 1, \Delta V_D = 0.025$) is assumed. **b** Profiles for the standard model, with varying Doppler broadening parameter $\Delta V_D = 0.0033, 0.0071, 0.0250$. These values correspond to Fe lines from a disk without turbulence ($\beta = 0$), with partly ($\beta = 0.29$) and with fully developed turbulence ($\beta = 1$). These Doppler widths can also be interpreted as being valid in non-turbulent disk for Fe, C, H lines. The line wings correspond to these three cases in reversed order (i.e. the "H" line profile is the uppermost one etc.). For comparison, the broken line marks the asymptotic line core without thermal broadening, $\Delta V_D = 0$

Central depth of a turbulent shell line is considerably increased as compared to the non-turbulent case,

$$F(V=0)/F_\star = 1 - H'^2_{sh} \quad (34)$$

(Fig. 10). The formulas for the approximate line profile at $V \neq 0$ in Eq. (30) remain valid, with $Y_{eff} \rightarrow H'_{sh}$ and $H_{sh} \rightarrow H'_{sh}$.

We note an important point, viz. that Fe shell lines in a turbulent disk with turbulence parameter β are identical to non-turbulent shell lines of species A with

$$A \approx \beta^{-2} \quad (35)$$

provided the same τ_0 applies. Especially, fully turbulent Fe shell lines correspond to *non-turbulent hydrogenic* shell lines, and the turbulent Fe shell lines of this section can be regarded as generalization of our approximation procedure to arbitrary species in non-turbulent disks.

Selected line profiles for our standard model in the limiting case $\beta = 1$ are shown in Fig. 11. Changes in the kinematical line wings are small and due to the modified H'_{sh}. Major modifications are observed in the *thermal*, now better called *turbulent* line core. The central peak has disappeared because central depth is given by $1 - H_{sh} \cdot Y_{eff}$ and Y_{eff} is of the order of H'_{sh} now. The central peak in Fig. 11 reveals to be characteristic of metallic ($\rightarrow$ low-ΔV_D), non-turbulent shell lines.

Table 3. Equivalent shell height H'_{sh} for turbulent Fe shell lines ($\beta = 1$), equivalent to non-turbulent H lines[a]

τ_0	H'_{sh}					
	$\alpha = 2$			$\alpha = 4$		
	$R_d = 5$	10	20	$R_d = 5$	10	20
10^{-1}	0.058	0.077	0.089	0	0	0
1	0.286	0.585	(1.06)	0.095	0.097	0.097
10	0.535	(1.31)	(3.12)	0.250	0.297	0.306
10^2	0.743	(1.94)	(4.98)	0.471	0.765	0.932
10^3	0.919	(2.46)	(6.53)	0.679	(1.39)	(2.33)
10^4	(1.07)	(2.91)	(7.86)	0.860	(1.97)	(4.10)
10^5	(1.21)	(3.31)	(9.04)	(1.02)	(2.48)	(5.73)

[a] Values in brackets (= $H'^\star_{sh}$) are used for interpolation (Sect. 4.2)

7. Conclusions

We have developed a model for shell absorption lines in Be stars, based on an isothermal Keplerian disk in hydrostatic equilibrium. We find that shell lines offer a unique opportunity to study a limited volume of a Be star disk, with typical fractional size of ≤ 10 %. Our analysis shows that the central depth of shell lines depends on two parameters, viz. the equivalent shell height H_{sh}, and the effective absorption width projected onto the stellar disk, Y_{eff}. This latter parameter is very sensitive to the intrinsic Doppler width of the line, i.e. on thermal and turbulent broadening. Beyond the thermal core velocity V_{thc} corresponding to Y_{eff}, the line profile is dominated by large-scale kinematic broadening in the disk. There exists a further critical velocity, V_d, determined by the outer disk radius, at which the line profile

may become deeper than at its centre, thus causing a central peak.

We have found that non-turbulent metallic shell lines can only obtain considerable depth (deeper than 0.75) if the disk is quite extended ($R_d \geq 10$). This is true for both density laws investigated here. Turbulent metallic shell lines are predicted to become much deeper even for small disk radii.

The thermal core may in principle be used to measure the Doppler width, i.e. the amount of turbulence persistent in the disk. This turbulence is then a direct measure of viscosity which is expected to drive matter in the disk back onto the star (self-accretion scenario for Be star disks, see Hanuschik et al. 1993).

Profiles of observed metallic shell lines fall into three classes: a) broad and symmetric, b) narrow and symmetric, c) broad and asymmetric. One can speculate that shell line profiles of the first class mainly show the broad kinematical part, with the central thermal peak being suppressed by turbulence. The second class seems to belong to very extended disks without turbulence in the outer parts, thus causing a deep narrow thermal core. The third class, because of its asymmetry, cannot be treated with our present model which predicts necessarily symmetric line profiles. This is definitely the domain of numerical modeling which will be the topic of a forthcoming paper. Similarly a deepergoing comparison of observed and modeled line profiles will follow.

Acknowledgements. I would like to thank Dr. Wolfgang Hummel for many fruitful discussions.

References

Dachs J., 1987, in *Physics of Be stars*, IAU Coll. 92, eds. A. Slettebak and T.P. Snow, Cambridge University Press, p. 149
Dachs J., Hummel W., Hanuschik R.W., 1992, A&AS, 95, 437
Doazan, V., 1987, in *Physics of Be stars*, IAU Coll. 92, eds. A. Slettebak and T.P. Snow, Cambridge University Press, p. 384
Frank J., King A., Raine D., 1992, *Accretion power in astrophysics* (2^{nd} ed.), Cambridge Univ. Press, Cambridge
Hanuschik R.W., 1988, A&A, 190, 187
Hanuschik R.W., 1989, Ap&SS, 161, 61
Hanuschik R.W., 1994, in *Pulsation, rotation and mass loss in early-type stars*, IAU Symp. 162, eds. L.A. Balona, H.F. Henrichs, J.M. LeContel, Kluwer, p. 358
Hanuschik R.W., Kozok J., Kaiser D., 1988, A&A, 189, 147
Hanuschik R.W., Dachs J., Baudzus M., Thimm G., 1993, A&A, 274, 356
Higurashi, T., Hirata, R., 1978, PASJ, 30, 615
Hirata, R., Kogure, T., 1978, PASJ, 30, 601
Horne K., Marsh T., 1986, MNRAS, 218, 761
Huang S.S., 1972, ApJ, 171, 549
Hummel W., Dachs J., 1992, A&A, 262, L17
Kogure T., 1975, PASJ, 27, 165
Pringle J., 1981, ARA&A, 19, 137
Slettebak A., Collins G.W., Truax, R., 1992, ApJS, 81, 335
Sobolev V.V., 1960, *Moving envelopes of stars*, Harvard Univ. Press, pp. 36

This article was processed by the author using Springer-Verlag LaTeX A&A style file version 3.